

Spectrum and thermal fluctuations of a microcavity polariton Bose-Einstein condensate

D. Sarchi* and V. Savona

Institute of Theoretical Physics, Ecole Polytechnique Fédérale de Lausanne EPFL, CH-1015 Lausanne, Switzerland

(Received 7 August 2007; revised manuscript received 10 October 2007; published 7 January 2008)

The Hartree-Fock-Popov theory of interacting Bose particles is developed, for modeling exciton-polaritons in semiconductor microcavities undergoing Bose-Einstein condensation. A self-consistent treatment of the linear exciton-photon coupling and of the exciton nonlinearity provides a thermal equilibrium description of the collective excitation spectrum, of the polariton energy shifts and of the phase diagram. Quantitative predictions support recent experimental findings.

DOI: [10.1103/PhysRevB.77.045304](https://doi.org/10.1103/PhysRevB.77.045304)

PACS number(s): 71.36.+c, 03.75.Nt, 42.65.-k, 71.35.Lk

I. INTRODUCTION

A major advance in the research on quantum fluids was made with the recent experimental observation of quantum degeneracy and off-diagonal long-range order (ODLRO), in a gas of exciton-polaritons in a semiconductor microcavity.¹⁻⁴ Bose-Einstein condensation (BEC) is the most appealing way of interpreting these findings. However, the 2D nature of the system, the presence of disorder, the hybrid exciton-photon composition of polaritons, and the composite nature of excitons call for models that account for the peculiar aspects of the polariton gas. Along this line, recent theoretical works have been successful in describing many specific aspects of the system. Disorder at the quantum well interfaces, in particular, was accounted for by a BCS-like theory in which bound excitons were modeled as particle-hole excitations coupled to the photon field.⁵⁻⁷ For strong exciton disorder, this theory models the density dependence of the polariton spectrum and shows how the linear optical response can probe successfully the phase transition. More generally, in presence of localization, the lower-energy region of the density of states is modified with respect to an ideal 2D system,^{8,9} making BEC of a trapped polariton gas the most suited description of the system. Finally, the short radiative lifetime of polaritons results in nonequilibrium effects,^{7,10-15} leading to condensate depletion¹⁵ and to a modified excitation spectrum.^{7,14} These effects should however be weak at densities above the condensation threshold,^{2,4} and are expected to be negligible for a polariton lifetime longer than 10 ps.³² Very recent measurements clearly show that thermal equilibrium polariton BEC can indeed be achieved.³ In spite of the high relevance of the existing theoretical frameworks, a basic question remains still unanswered. Are the experimental findings correctly interpreted in terms of a quantum field theory of interacting bosons? Such a theory should account self-consistently for the linear coupling between two Bose fields—photons and excitons—and for the Coulomb and Pauli nonlinearities arising from the composite nature of excitons.

In this work, we answer this question by generalizing the Hartree-Fock-Popov (HFP)^{16,17} theory of BEC to the case of two coupled Bose fields. In order to address the fundamental thermodynamical properties of the polariton gas, we assume thermal equilibrium—as was done in previous works based on nonbosonic models^{5,6}—and discuss kinetic effects else-

where.¹⁵ We address the problem of BEC of a confined 2D system, i.e., the regime expected to be relevant for current experiments, while the problem of quasicondensation of an extended system will be treated in a future publication. The system, including the Coulomb and Pauli nonlinear exciton terms, is described within an effective boson Hamiltonian,¹⁸⁻²⁰ valid well below the exciton Mott density. We derive coupled equations for the condensate wave function and the field of excitations, and study the solutions for parameters modeling a recent experiment.² We discuss the collective excitation spectrum, the density-dependent energy shifts, the onset of off-diagonal long-range order and the phase diagram. Our analysis provides a generally good account of the experimental findings, in particular by reproducing the measured critical density and the energy shifts of the two polariton modes.

II. THEORY

Let us introduce the exciton and photon operators \hat{b}_k and \hat{c}_k , obeying Bose commutation rules.³³ The polariton Hamiltonian then reads

$$\hat{H} = \hat{H}_0 + \hat{H}_R + \hat{H}_x + \hat{H}_s, \quad (1)$$

where $\hat{H}_0 = \sum_{\mathbf{k}} \epsilon_{\mathbf{k}}^{\dagger} \hat{b}_{\mathbf{k}}^{\dagger} \hat{b}_{\mathbf{k}} + \epsilon_{\mathbf{k}}^c \hat{c}_{\mathbf{k}}^{\dagger} \hat{c}_{\mathbf{k}}$ is the noninteracting term, $\hat{H}_R = \hbar \Omega_R \sum_{\mathbf{k}} (b_{\mathbf{k}}^{\dagger} \hat{c}_{\mathbf{k}} + \text{H.c.})$ describes the linear exciton-photon coupling, and $\hat{H}_x = \frac{1}{2} \sum_{\mathbf{k}\mathbf{k}'\mathbf{q}} v_x(\mathbf{k}, \mathbf{k}', \mathbf{q}) \hat{b}_{\mathbf{k}+\mathbf{q}}^{\dagger} \hat{b}_{\mathbf{k}'-\mathbf{q}}^{\dagger} \hat{b}_{\mathbf{k}} \hat{b}_{\mathbf{k}'}$ is an effective two-body exciton Hamiltonian, modeling both Coulomb interaction and the effect of Pauli exclusion on electrons and holes. The term $\hat{H}_s = \sum_{\mathbf{k}\mathbf{k}'\mathbf{q}} v_s(\mathbf{k}, \mathbf{k}', \mathbf{q}) (\hat{c}_{\mathbf{k}+\mathbf{q}}^{\dagger} \hat{b}_{\mathbf{k}'-\mathbf{q}}^{\dagger} \hat{b}_{\mathbf{k}} \hat{b}_{\mathbf{k}'} + \text{H.c.})$ models the effect of Pauli exclusion on the exciton oscillator strength,^{18,20} which decreases for increasing exciton density.²² We account for the full momentum dependence of $v_x(\mathbf{k}, \mathbf{k}', \mathbf{q})$ and $v_s(\mathbf{k}, \mathbf{k}', \mathbf{q})$.^{18,20} They vanish at large momenta, preventing the ultraviolet divergence typical of a contact potential.^{23,34} For clarity, however, we use the short form $v_x(\mathbf{k}, \mathbf{k}', \mathbf{q}) \rightarrow v_x$ and $v_s(\mathbf{k}, \mathbf{k}', \mathbf{q}) \rightarrow \hbar \Omega_R / n_s$ in what follows, where n_s is the saturation density of the exciton oscillator strength.¹⁸

As noninteracting exciton and photon modes, we assume states in a square box of area A with periodic boundary conditions. In real microcavities, interface fluctuations affect the photon modes, resulting in a disorder potential and in polar-

iton localization over a few μm^2 . For equilibrium BEC, the energy spacings between the lowest-lying states determine locally the effect of quantum fluctuations. Our finite size assumption thus models in a simple way the local structure of the spectrum of the disordered system. We anticipate that the results manifest a weak (logarithmic) dependence on the system size A (see Fig. 5), as expected for a 2D system.

Via the Bogoliubov ansatz, the exciton and the photon fields are written as

$$\hat{\Psi}_{x,c}(\mathbf{r},t) = \Phi_{x,c}(\mathbf{r},t) + \tilde{\psi}_{x,c}(\mathbf{r},t), \quad (2)$$

i.e., as the sum of a classical symmetry-breaking term $\Phi_{x,c}(\mathbf{r},t)$ for the condensate wave function, and of a quantum fluctuation field $\tilde{\psi}_{x,c}(\mathbf{r},t)$. Heisenberg equations of motion result in two coupled equations for $\Phi_{x,c}(\mathbf{r},t)$. In the HFP approach, anomalous correlations of the excitation field are neglected^{16,17} and we obtain

$$\begin{aligned} i\hbar\dot{\Phi}_x &= \left[\epsilon_0^x - 2\frac{\hbar\Omega_R}{n_s} \text{Re}\{n_{xc} + \tilde{n}_{xc}\} + v_x(n_{xx} + \tilde{n}_{xx}) \right] \Phi_x \\ &+ \hbar\Omega_R \left(1 - \frac{n_{xx}}{n_s} \right) \Phi_c, \\ i\hbar\dot{\Phi}_c &= \epsilon_0^c \Phi_c + \hbar\Omega_R \left(1 - \frac{n_{xx} + \tilde{n}_{xx}}{n_s} \right) \Phi_x. \end{aligned} \quad (3)$$

Here, we introduce the density matrix $n_{\chi\xi} = n_{\chi\xi}^0 + \tilde{n}_{\chi\xi}$ ($\chi, \xi = x, c$), where $n_{\chi\xi}^0 = \Phi_{\chi}^* \Phi_{\xi}$ and $\tilde{n}_{\chi\xi} = \sum_{\mathbf{k} \neq 0} n_{\chi\xi}(\mathbf{k}) = \sum_{\mathbf{k} \neq 0} \langle \hat{O}_{\chi}^2(\mathbf{k}) \hat{O}_{\xi}^1(\mathbf{k}) \rangle$ are the contributions from the condensate and from the excited states, respectively. In our notation, $\hat{O}_{\xi}^1(\mathbf{k}) = \hat{O}_{\xi}(\mathbf{k})$ and $\hat{O}_{\xi}^2(\mathbf{k}) = \hat{O}_{\xi}^{\dagger}(-\mathbf{k})$, with $\hat{O}_x = \hat{b}$, and $\hat{O}_c = \hat{c}$. The quantities $n_{\chi\xi}(\mathbf{k})$ are computed self-consistently as described below. By setting $\Phi_{x,c}(t) = e^{-i\mu t/\hbar} \Phi_{x,c}(0)$ into Eq. (3), we obtain a generalized set of two coupled Gross-Pitaevskii equations for the condensate eigenstate. The two solutions of Eq. (3) correspond to the lower and upper polariton respectively, and can be expressed as $\Phi_{up(lp)} = X_0^{up(lp)} \Phi_x + C_0^{up(lp)} \Phi_c$, thus fixing the Hopfield coefficients of the polariton condensate. The low-energy solution μ defines the chemical potential of the system.

In the HFP theory, Eqs. (3) are coupled to the field equations for excitations. In analogy with the standard description of a single Bose field,¹⁷ we define the 4×4 matrix $G(\mathbf{k}, i\omega_n) \equiv \{g_{jl}^{\chi\xi}(\mathbf{k}, i\omega_n)\}_{j,l=1,2}^{\chi,\xi=x,c}$, whose elements are the thermal propagators of the excited particles:¹⁷

$$g_{jl}^{\chi\xi}(\mathbf{k}, i\omega_n) = - \int_0^{\beta} d\tau e^{i\omega_n \tau} \langle \hat{O}_{\chi}^j(\mathbf{k}, \tau) \hat{O}_{\xi}^l(\mathbf{k}, 0)^{\dagger} \rangle_{\tau}, \quad (4)$$

where $\hbar\omega_n = 2\pi n/\beta$, $n=0, \pm 1, \dots$ are the Matsubara energies for bosons and $\langle \dots \rangle_{\tau}$ represents the thermal average of the imaginary-time ordered product.

The propagator matrix $G(\mathbf{k}, i\omega_n)$ obeys the Dyson-Belaev equation

$$G(\mathbf{k}, i\omega_n) = G^0(\mathbf{k}, i\omega_n) [\mathbf{1} + \Sigma(\mathbf{k}, i\omega_n) G(\mathbf{k}, i\omega_n)], \quad (5)$$

where

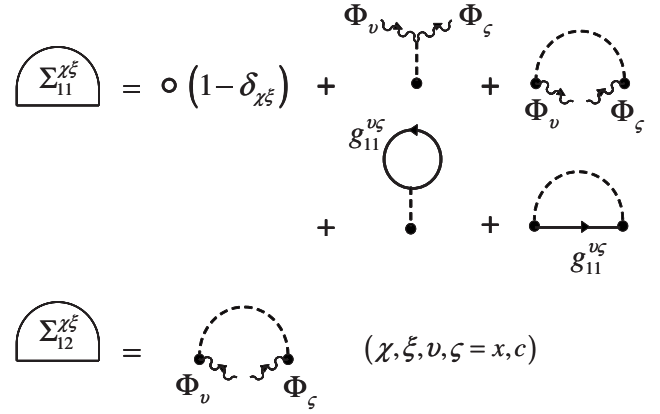


FIG. 1. Diagrammatic representation of the HFP self-energy Eq. (8). Wiggly lines represent the condensate fields Φ_v while thick solid lines represent the self-consistent many-body propagators of excitations $g_{11}^{v\xi}$ ($v, \xi = x, c$). The open circle in the equation for $\Sigma_{11}^{\chi\xi}$ represents the scattering of an exciton into a photon and vice versa, due to the linear coupling \hat{H}_R . The sum over the labels v and ξ is implicitly assumed. Dashed lines represent the two-body interaction $v = v_x$ or $v = v_s$, depending on the diagram considered, according to the relation $v = \delta_{\chi\xi} \delta_{\chi x} [\delta_{v\xi} \delta_{v_x} v_x + (1 - \delta_{v\xi}) v_s] + (1 - \delta_{\chi\xi}) \delta_{v\xi} \delta_{v_x} v_s$. Notice that, due to the structure of \hat{H}_s , the only admitted diagrams are those for which no more than one photon label c appears.

$$G^0 \equiv \{g_{jl}^0(\mathbf{k}, i\omega_n)\}_{jl}^{\chi\xi} = \frac{\delta_{\chi\xi} \delta_{jl}}{(-)i\omega_n - \epsilon_{\mathbf{k}}^{(\xi)} + \mu} \quad (6)$$

is the matrix of the unperturbed propagators, and

$$\Sigma(\mathbf{k}, i\omega_n) = \begin{pmatrix} \Sigma^{xx}(\mathbf{k}, i\omega_n) & \Sigma^{xc}(\mathbf{k}, i\omega_n) \\ \Sigma^{cx}(\mathbf{k}, i\omega_n) & \Sigma^{cc}(\mathbf{k}, i\omega_n) \end{pmatrix} \quad (7)$$

is the 4×4 self-energy matrix, here written in a (2×2) -block form. In the HFP limit, the self-energy is independent of frequency and reads

$$\Sigma_{11}^{xx} = \Sigma_{22}^{xx} = 2 \left[v_x n_{xx} - \frac{\hbar\Omega_R}{n_s} (n_{cx} + n_{xc}) \right],$$

$$\Sigma_{12}^{xx} = (\Sigma_{21}^{xx})^* = v_x \Phi_x^2 - 2 \frac{\hbar\Omega_R}{n_s} \Phi_x \Phi_c,$$

$$\Sigma_{11}^{xc} = \Sigma_{22}^{xc} = \hbar\Omega_R \left(1 - 2 \frac{n_{xx}}{n_s} \right),$$

$$\Sigma_{12}^{xc} = (\Sigma_{21}^{xc})^* = - \frac{\hbar\Omega_R}{n_s} \Phi_x^2, \quad (8)$$

while $\Sigma_{jl}^{cx} = \Sigma_{jl}^{xc}$ and $\Sigma_{jl}^{cc} = 0$. The corresponding self-energy diagrams are sketched in Fig. 1. For each value of \mathbf{k} , the analytic continuation of the Green's functions $g_{jl}^{\chi\xi}(\mathbf{k}, z)$ have four poles at $z = \pm E_{\mathbf{k}}^{lp(up)}$. They are the positive and negative eigen-energies of the lower- and upper-polariton Bogoliubov modes. The components of the corresponding eigenvectors $\mathbf{h}_{\sigma}^i(k) \equiv (X_u, C_u, X_v, C_v)_{\sigma}^i(k)$ ($i = lp, up$ and $\sigma = +, -$) are the generalized Hopfield coefficients of the normal (X_u, C_u) and

anomalous (X_v, C_v) kind, with normalization $|X_u|^2 - |X_v|^2 + |C_u|^2 - |C_v|^2 = 1$.

The excited-state density matrix $\tilde{n}_{\chi, \xi}(\mathbf{k})$ is related to the normal Green's functions via the relations

$$\tilde{n}_{\chi, \xi}(\mathbf{k}) = \lim_{\eta \rightarrow 0} \sum_{\omega_n} e^{i\omega_n \eta} g_{11}^{\chi, \xi}(\mathbf{k}, i\omega_n). \quad (9)$$

The corresponding lower- and upper-polariton densities $\tilde{n}_{lp}(\mathbf{k})$ and $\tilde{n}_{up}(\mathbf{k})$ are obtained from Eq. (9) in terms of the generalized Hopfield coefficients. Thus, for a fixed total polariton density n_p , the condensed lower-polariton population is given by

$$n_{lp}^0 \equiv |\Phi_{lp}|^2 = n_p - \tilde{n}_{lp} - \tilde{n}_{up}. \quad (10)$$

From this quantity, Φ_x and Φ_c are finally obtained via the Hopfield coefficients for the condensate X_0 and C_0 , as derived from Eq. (3). Hence a fully self-consistent solution can be obtained by solving iteratively Eqs. (3), (5), (9), and (10), until convergence of the chemical potential μ and of the density matrix $n_{\chi, \xi}(\mathbf{k})$ is reached. From this solution, for a given polariton density n_p , temperature T , and system size A , we obtain the spectrum of collective excitations $E_{\mathbf{k}}^{lp(up)}$ and the polariton population $n_{lp(up)}(\mathbf{k})$.

We stress that the present formalism directly applies only to a finite system. In particular, Eq. (9) is well defined only for a finite area A , while it is infrared-divergent in the thermodynamic limit ($A \rightarrow \infty$), if a condensate exists. This behavior is due to the divergence of phase fluctuations, and it is responsible for the occurrence of quasicondensation in place of BEC in a 2D extended system.^{23,28,29} Since in the present work we address conventional BEC of a confined gas (i.e., we always consider finite areas), it is not strictly necessary to separate density and phase fluctuations. However, for completeness, we sketch in Appendix A a possible extension of the present formalism where we separate the two contributions. The results reported in Appendix A support our choice, suggesting that phase fluctuations could be possibly dominant (resulting in quasicondensation) only for an area A two orders of magnitude larger than the typical area of confined polaritons in current experiments.

III. RESULTS AND DISCUSSION

For the numerical calculations, we use parameters describing the experiment in Ref. 2, i.e., $\hbar\Omega_R = 13$ meV and detuning $\delta = \epsilon_0^c - \epsilon_0^x = 5$ meV. We study the results as a function of the system area A , ranging from $100 \mu\text{m}^2$ to 1cm^2 . The momentum-dependent interaction potentials v_x and v_s ,¹⁸ are evaluated for a CdTe quantum well, for which the exciton binding energy is $E_b = 25$ meV, the exciton Bohr radius is $a_0 = 4.7$ nm and the effective masses of the electron and the hole are $m_{el} = 0.096 m_0$ and $m_h = 0.2 m_0$, respectively, m_0 being the electron mass.

At temperatures sufficiently lower than the critical temperature T_c , i.e., $T \leq 0.5T_c$, the HFP approximation (and, under more restrictive conditions, even the Bogoliubov approximation) has been found to reproduce fairly well the thermodynamics^{26,27} and the excitation spectrum²⁵ of a 3D

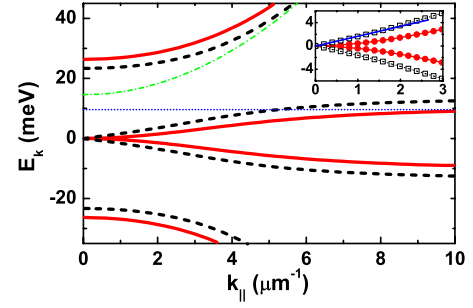


FIG. 2. (Color online) The dispersion of the normal modes of the system for $T=20$ K, $A=1000 \mu\text{m}^2$ and polariton density $n_p = 15 \mu\text{m}^{-2}$ (solid) and $n_p = 400 \mu\text{m}^{-2}$ (dashed). The noninteracting photon (dash-dotted) and exciton (dotted) modes are also shown. Inset: Detail of the low-energy region (points and squares denote the actual k discrete states obtained in our finite-size calculation), showing the onset of the linear Bogoliubov dispersion (the blue straight line is a guide to the eye).

weakly interacting Bose gas.²⁵ Furthermore, higher order effects of fluctuations are expected to produce a correction of a few percent also in the limiting case of an infinite 2D system.²⁹ Hence, given also the limited experimental accuracy in determining the polariton temperature and density, the HFP theory is expected to give realistic predictions of the measured data. Below, we will study the region of the phase diagram in which the thermal fluctuations, included to the lowest order in the HFP theory, are essential in determining the phase boundary.

In Fig. 2 we show the energy-momentum dispersion of the collective excitations, $\pm E_{\mathbf{k}}^{lp}$ and $\pm E_{\mathbf{k}}^{up}$, as obtained for two different values of the total polariton density n_p above the condensation threshold, at $T=20$ K. Close to zero momentum (see inset), the dispersion of the lower polariton branch becomes linear, giving rise to phononlike Bogoliubov modes,^{6,21} as in the standard single-field theory.²³ Due to the nonlinear terms \hat{H}_x and \hat{H}_s , the polariton splitting decreases for increasing n_p .

The interplay between exciton saturation and interactions in determining the energy shifts has no counterpart in the BEC of a single Bose gas. Here, the two effects produce *independent* energy shifts of the two polaritons. We plot in Fig. 3(a) the energy shifts of the two polariton modes at $k=0$, as a function of the density. Exciton saturation and interactions result in a blueshift of the lower polariton and a redshift of the upper polariton. The shifts are linear in n_p with the slope changing by a factor of two across the threshold (see inset), because the contribution of the thermal populations $\tilde{n}_{xx}, \tilde{n}_{xc}$ in Eqs. (3) is twice that of the condensed ones n_{xx}^0, n_{xc}^0 . This trend and the magnitude of the shifts reproduce fairly well the experimental data.² To explain the origin of the opposite shifts of the two polaritons, we plot in Fig. 3(b) the exciton energy $E_0^x \equiv \epsilon_0^x + \sum_{11}^{xx}$, and the exciton-photon coupling \sum_{11}^{xc} , as a function of n_p . The two quantities contribute comparably to the deviations from the ideal Bose-gas picture. We predict a very small reduction of the polariton splitting up to the largest polariton density estimated from the experiments, thus supporting the idea that polaritons—as hy-

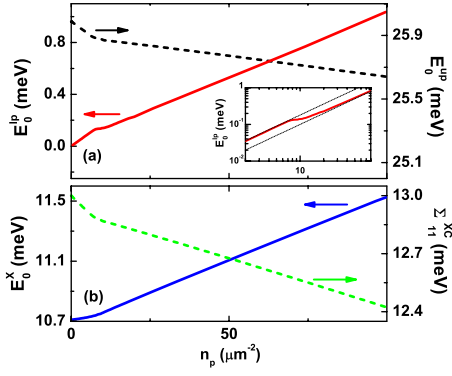


FIG. 3. (Color online) (a) Lower (solid) and upper (dashed) polariton energies at $k=0$ vs polariton density n_p . Inset: Double logarithmic plot of the lower polariton energy (dotted lines: linear slopes below and above threshold). (b) Bare exciton energy E_0^x (solid) and effective exciton-photon coupling Σ_{11}^{xc} (dashed). All quantities were computed for $T=20$ K and $A=100 \mu\text{m}^2$.

brid exciton-photon quasiparticles—are stable well above the BEC threshold.

We now turn to study the thermodynamical properties of polariton BEC. Figure 4(a) shows the energy distribution of the polariton population $n_{lp}(E)+n_{up}(E)$ for three values of the total density n_p , well below, just below, and above the critical density. In the first case, polaritons follow a Maxwell-Boltzmann distribution. For increasing density, the distribution becomes degenerate at low energy. Due to confinement and to the resulting discrete energy spectrum, a density threshold exists above which the population in the $\mathbf{k} \neq 0$ saturates and the system condenses in the lowest-energy state at $\mathbf{k}=0$. This behavior accounts very well for the data measured in recent experiments.^{2,4} In the inset of Fig.

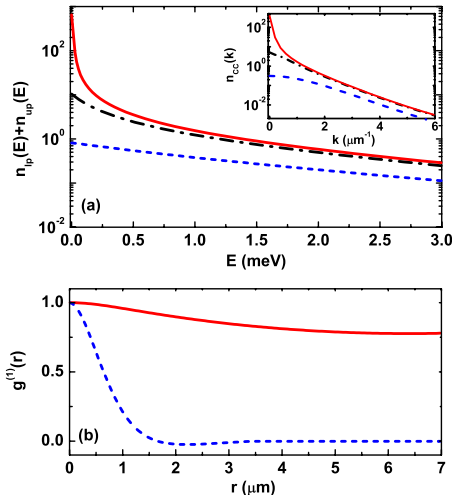


FIG. 4. (Color online) (a) Polariton population vs energy, computed at $T=20$ K and for $A=100 \mu\text{m}^2$, for $n_p=3 \mu\text{m}^{-2}$ (dashed line), $n_p=7 \mu\text{m}^{-2}$ (dash-dotted line) and $n_p=15 \mu\text{m}^{-2}$ (solid line). The system is condensed only for $n_p=15 \mu\text{m}^{-2}$. In the inset, we display the corresponding momentum distribution of photons. (b) One-body spatial correlation function of the photon field for $n_p=3 \mu\text{m}^{-2}$ (dashed line) and for $n_p=15 \mu\text{m}^{-2}$ (solid line).

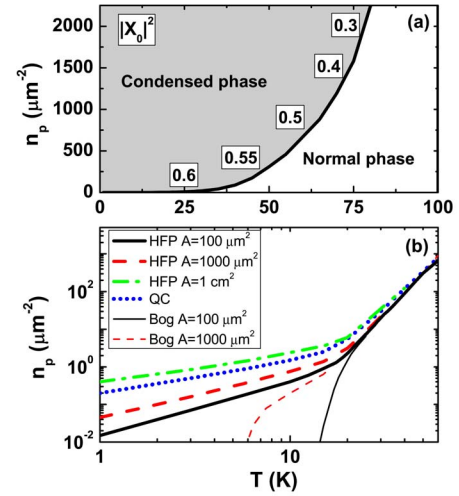


FIG. 5. (Color online) (a) Phase diagram of polariton BEC, computed for the parameters of Ref. 2, and $A=100 \mu\text{m}^2$. The exciton fraction in the condensate $|X_0|^2$, along the phase boundary, is indicated in boxes. (b) Detail of the low- T region. ‘‘HFP’’ denotes the result of the present theory. ‘‘Bog’’ is the result of the Bogoliubov limit. ‘‘QC’’ denotes the quasi-condensate transition, corresponding to the onset of a superfluid density.

4(a) we display the corresponding momentum distribution of photons, $n_{cc}(k)$ —another quantity that can be extracted from experiments. This quantity is particularly relevant for systems that are not strongly dominated by disorder,^{1,3,4} and is the one directly related to the one-body spatial correlation function of the photon field

$$g^{(1)}(\mathbf{r}) = \langle \hat{\psi}_c^\dagger(\mathbf{r}) \hat{\psi}_c(0) \rangle / [n_{cc}(\mathbf{r}) n_{cc}(0)]^{1/2}, \quad (11)$$

which is displayed in Fig. 4(b).³⁵ This function is directly related, via the photon fraction, to the actual polariton correlation function, and models the outcome of an optical experiment. It shows the occurrence of ODLRO above threshold which is the main feature of BEC of an interacting Bose gas.²³ Below threshold, the correlation extends only over the thermal wavelength $\lambda_T \approx 1 \mu\text{m}$. This value reproduces the spatial extension of coherence in the non-condensed regime, measured in recent experiments.^{2,4} For condensed polaritons, on the other hand, our theory predicts correlations that extend over the whole system size. This is also observed in experiments,^{2,4} where the spatial region of high correlation has a pattern determined by the shape of the underlying disorder potential.² However, the measured long-range correlation is always below 40%, as compared to 80% of our prediction. By means of a kinetic model, we have recently suggested¹⁵ that this discrepancy is the main result of deviations from thermodynamical equilibrium, with enhanced fluctuations depleting the condensate in favor of excitations.

In Fig. 5(a), we report the computed density-temperature phase diagram. In the plot, some values of the exciton fraction $|X_0|^2$ in the polariton condensate are indicated along the phase boundary. It decreases for increasing density, due to interactions, but stays finite, confirming the stability of polaritons up to high density. Figure 5(b) shows a detail of the

low- T region of the phase diagram, computed for different system areas A .

To make a quantitative comparison with experimental findings, two points should be clarified. First, what is measured in experiments is the population of the optically active polariton states, i.e., states having a nonvanishing photon fraction. Indeed, an optical measurement cannot directly assess the excitonlike region of the polariton spectrum at high energy. Second, we know that the occupation of high energy modes is expected to be larger than the thermal equilibrium estimate, due to kinetic effects.^{12,15} Therefore, the critical density that we predict is a lower bound to the total density (including excitonlike regions of the spectrum) required for condensation in a regime of steady-state pumping. This said, at $T \approx 20$ K our theory predicts a density threshold $n_p \approx 3-10 \mu\text{m}^{-2}$ for system sizes ranging from $A = 100 \mu\text{m}^2$ to $A = 1 \text{cm}^2$. These values agree very well with the measured polariton density at the BEC threshold $n_{\text{th}} \approx 5 \mu\text{m}^{-2}$, at a measured polariton temperature $T \approx 20$ K, as reported by Kasprzak and co-workers.²

The thin lines in Fig. 5(b) are the result of the Bogoliubov approximation, obtained by assuming that in the condensed regime all the particles are in the condensate. This corresponds to set $n_{\chi\xi}^0 = n_{\chi\xi}$ and $\tilde{n}_{\chi\xi} = 0$ in Eqs. (3) and (8). This approximation overestimates the group velocity of the excitations, thus underestimating considerably the critical density at low temperature. The comparison between the Popov and the Bogoliubov lines shows that the role of fluctuations becomes relevant for temperatures below $T = 20$ K and for densities below $3 \mu\text{m}^{-2}$. Clearly, in this region of the phase diagram the Popov approximation is required to provide realistic predictions. Within the different context of a Fermi-Bose theory, Keeling *et al.* have come to similar conclusions.⁵

In Fig. 5(b) we also display the phase boundary of the normal-superfluid (quasicondensate) transition. This boundary has been already computed by Kavokin *et al.*⁸ by adopting the Landau criterion²³ for the lower polariton field. However, as it has been recently shown by Keeling,⁹ if $k_B T$ is close to the polariton splitting, a direct application of the Landau criterion to a nonquadratic dispersion might lead to an inconsistency, and a different superfluid criterion is required. Here we estimate the phase boundary by imposing that, in the superfluid regime, both the exciton and the photon superfluid densities are nonvanishing and by adopting the Landau formula²³ for both fields. The details of the derivation are reported in the Appendix B, while the more general problem of the superfluid properties of polaritons will be the object of future work. We notice that the phase boundary obtained within the present theory agrees with the ones reported in Refs. 8 and 9.

For $T < 20$ K and A ranging between $A = 100 \mu\text{m}^2$ and $A = 1000 \mu\text{m}^2$, the BEC critical density is lower than the normal-superfluid one, and the difference significantly increases for decreasing temperatures. Our BEC picture is thus well suited for the description of recent samples,²⁻⁴ characterized by polariton localization. In the case of a more extended, spatially homogeneous system, a description in terms of the Berezinski-Kosterlitz-Thouless (BKT) transition would be necessary. Figure 5(b) also shows the logarithmic

increase of the critical density as a function of A , due to the increase of thermal fluctuations. Quantitatively, the variation is very small, in particular for $T \geq 20$ K. This dependence and the quasicondensate behaviour are hence only expected in samples with improved interface quality and at lower temperature.

IV. CONCLUSIONS

In conclusion, we have generalized the HFP theory to the case of two coupled Bose fields at thermal equilibrium. The theory allows modeling the BEC of polaritons in semiconductor microcavities in very close analogy with the BEC of a weakly interacting gas. The predicted critical density is in good agreement with a recent measurement.² Our analysis thus supports the interpretation of the experimental findings in terms of a transition to a quantum degenerate Bose fluid. Open questions remain, basically related to the role of disorder and localization. If the sample quality can be improved, polaritons will become an invaluable tool for studying the effects of dimensionality and fluctuations in interacting Bose systems.

ACKNOWLEDGMENTS

We acknowledge financial support from the Swiss National Foundation through Grant No. PP002-110640.

APPENDIX A: PHASE AND DENSITY FLUCTUATIONS

In this appendix, we outline how a proper account of phase fluctuations in the thermodynamic limit can be given by extending the standard method described in Refs. 23, 28, and 29. We also show that the power-law decay of the first order correlation functions $g^{(1)}(\mathbf{r})$ is expected to occur over distances much larger than the typical confinement length.

To separate density and phase fluctuations, it is useful to express the exciton and photon fields in terms of the Bogoliubov polariton modes ($j=1, \dots, 4$)

$$\hat{\pi}_{\mathbf{k}}^{(j)} = X_u^{(j)}(\mathbf{k})\hat{b}_{\mathbf{k}} + X_v^{(j)}(\mathbf{k})\hat{b}_{-\mathbf{k}}^\dagger + C_u^{(j)}(\mathbf{k})\hat{c}_{\mathbf{k}} + C_v^{(j)}(\mathbf{k})\hat{c}_{-\mathbf{k}}^\dagger, \quad (\text{A1})$$

here expressed in terms of the generalized Hopfield coefficients. By inverting Eq. (A1), we write the exciton and the photon operators as

$$\begin{aligned} \hat{b}_{\mathbf{k}} &= \Pi_u^x(\mathbf{k})\hat{\pi}_{\mathbf{k}} + \Pi_v^x(\mathbf{k})\hat{\pi}_{-\mathbf{k}}^\dagger + \Omega_u^x(\mathbf{k})\hat{\omega}_{\mathbf{k}} + \Omega_v^x(\mathbf{k})\hat{\omega}_{-\mathbf{k}}^\dagger, \\ \hat{c}_{\mathbf{k}} &= \Pi_u^c(\mathbf{k})\hat{\pi}_{\mathbf{k}} + \Pi_v^c(\mathbf{k})\hat{\pi}_{-\mathbf{k}}^\dagger + \Omega_u^c(\mathbf{k})\hat{\omega}_{\mathbf{k}} + \Omega_v^c(\mathbf{k})\hat{\omega}_{-\mathbf{k}}^\dagger, \end{aligned} \quad (\text{A2})$$

where $\hat{\pi} = \hat{\pi}^{(1)}$ represents the positive-weighted lower-polariton mode while $\hat{\omega} = \hat{\omega}^{(3)}$ represents the positive-weighted upper-polariton mode. From there, the photon (or, analogously, the exciton) population can be written as

$$\begin{aligned}
\tilde{n}_{cc} &= \sum_{\mathbf{k} \neq 0} [|\Pi_u^c(\mathbf{k})|^2 + |\Pi_v^c(\mathbf{k})|^2] n_B(E_{\mathbf{k}}^{lp}) + |\Pi_v^c(\mathbf{k})|^2 \\
&\quad + (|\Omega_u^c(\mathbf{k})|^2 + |\Omega_v^c(\mathbf{k})|^2) n_B(E_{\mathbf{k}}^{up}) + |\Omega_v^c(\mathbf{k})|^2 \\
&\equiv \sum_{\mathbf{k} \neq 0} \frac{P^c}{E_{\mathbf{k}}^{lp}} n_B(E_{\mathbf{k}}^{lp}) + D_{\pi}^c(\mathbf{k}) + D_{\omega}^c(\mathbf{k}), \quad (\text{A3})
\end{aligned}$$

where, in the last line, we have defined three terms, i.e., the contribution from the upper-polariton modes (free of infrared divergences)

$$D_{\omega}^c(\mathbf{k}) = [|\Omega_u^c(\mathbf{k})|^2 + |\Omega_v^c(\mathbf{k})|^2] n_B(E_{\mathbf{k}}^{up}) + |\Omega_v^c(\mathbf{k})|^2, \quad (\text{A4})$$

the contribution from the lower-polariton phase fluctuations (infrared-divergent), defined via the limit

$$P^c \equiv \lim_{k \rightarrow 0} \frac{E_{\mathbf{k}}^{lp}}{n_B(E_{\mathbf{k}}^{lp})} \tilde{n}_{cc}(\mathbf{k}) = \lim_{k \rightarrow 0} k^2 \tilde{n}_{cc}(k), \quad (\text{A5})$$

and the contribution due to the lower-polariton density fluctuations, defined by the difference

$$D_{\pi}^c(\mathbf{k}) = \tilde{n}_{cc}(\mathbf{k}) - D_{\omega}^c(\mathbf{k}) - \frac{P^c}{E_{\mathbf{k}}^{lp}} n_B(E_{\mathbf{k}}^{lp}). \quad (\text{A6})$$

We notice that, to define phase fluctuations, we have extracted the divergent part of excitations (proportional to k^{-2}), thus extending the standard definition given in Refs. 23, 28, and 29.

By using the separation introduced in Eq. (A3) and generalizing the derivation of Ref. 28 to the present case, we write the one-body spatial correlation function for the photon field, defined in Eq. (11), as

$$g^{(1)}(\mathbf{r}) = e^{-\Lambda(\mathbf{r})} \tilde{\rho}(\mathbf{r}), \quad (\text{A7})$$

where the exponent function

$$\Lambda(\mathbf{r}) \equiv \frac{1}{n_{cc}} \sum_{\mathbf{k}} [1 - \cos(\mathbf{k} \cdot \mathbf{r})] \frac{P^c}{E_{\mathbf{k}}^{lp}} n_B(E_{\mathbf{k}}^{lp}) \quad (\text{A8})$$

is associated with phase fluctuations. This quantity increases with \mathbf{r} and is responsible for the long-range power-law decay of correlations. The function

$$\tilde{\rho}(\mathbf{r}) = 1 - n_{cc}^{-1} \sum_{\mathbf{k}} [1 - \cos(\mathbf{k} \cdot \mathbf{r})] [D_{\pi}^c(\mathbf{k}) + D_{\omega}^c(\mathbf{k})], \quad (\text{A9})$$

on the other hand, is associated to density fluctuations and is expected to decay over distances much shorter than the phase-fluctuations decay length,²⁸ to the constant value

$$\frac{n_c^{\text{QC}}}{n_{cc}} \equiv \lim_{r \rightarrow \infty} \tilde{\rho}(\mathbf{r}), \quad (\text{A10})$$

which defines the quasicondensate fraction. We notice that, in order to treat quasicondensation in a self-consistent way, the quasicondensate density matrix should replace the condensate one in Eqs. (3) and (8), and a self-consistent solution should be computed,²⁸ as we did for BEC in a trap. This self-consistent approach goes beyond the scope of the present work.

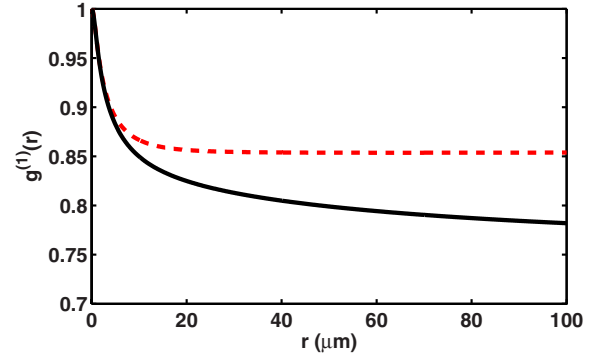


FIG. 6. (Color online) One-body spatial correlation function $g^{(1)}(r)$ (solid line), obtained for $T=20$ K, $n_p=10 \mu\text{m}^{-2}$, and $A=10^5 \mu\text{m}^2$. The condensate density (used to evaluate the energy dispersion $E_{\mathbf{k}}^{lp(up)}$) is $n_p^0=4 \mu\text{m}^{-2}$. The dashed line represents the contribution $\tilde{\rho}(r)$.

We have argued above, that the typical area of confinement for realistic polariton systems is sufficiently small to allow a description in terms of BEC of a spatially confined gas. To quantitatively justify this statement, in Fig. 6 we plot the function $g^{(1)}(\mathbf{r})$ and the function $\tilde{\rho}(\mathbf{r})$ for a very large system area $A=10^5 \mu\text{m}^2$. For this quantitative estimate, we have used the values of $E_{\mathbf{k}}^{lp(up)}$, $\Pi_u^{x(c)}(\mathbf{k})$, $\Pi_v^{x(c)}(\mathbf{k})$, $\Omega_u^{x(c)}(\mathbf{k})$, and $\Omega_v^{x(c)}(\mathbf{k})$, as obtained from Eqs. (5)–(8) and (A2), by assuming a condensate in a system with area $A=10^5 \mu\text{m}^2$, instead of accounting in a self-consistent way for the quasicondensate density matrix. However, for this value of A , we find that the quasicondensate density matrix, as obtained from Eq. (A10), differs from the condensate one by less than 10%, the discrepancy becoming considerable only for much larger areas. The comparison in Fig. 6 clearly shows that, while the short-range decay due to density fluctuations is over distances of the order of few μm , the long-range decay due to phase fluctuations is over distances of the order of hundreds of μm , i.e., one order of magnitude larger than the typical confinement length.^{30,31} This analysis thus suggests that, under typical experimental conditions, the effect of phase fluctuations in determining the correlation properties, and thus the occurrence of quasicondensation, can be safely neglected. On the other hand, a more specific analysis of the occurrence of vortices, would be required to assess whether the BKT crossover might occur in place of BEC. Indeed, configurations with one or more vortices are expected to become entropically favored if the vortex size is sufficiently smaller than the system size.²³ Here, we only give a rough estimate of the vortex core size which, for a uniform system, is given by the healing length.²³ The healing length of polaritons is defined as $\xi(n_p) = \hbar / \sqrt{m_{\text{pol}} v n_p}$,¹⁵ where $m_{\text{pol}} \simeq 7 \times 10^{-5} m_0$ is the effective mass of lower polaritons at $k=0$, m_0 the electron mass, and $v = (v_x X_0 + \hbar \Omega_R / n_s |C_0|) X_0^3 \simeq 2 \times 10^{-3} \text{ meV } \mu\text{m}^2$ is the effective two-body interaction at $k=0$. At a density $n_p \simeq 10 \mu\text{m}^{-2}$, we find $\xi(n_p) \simeq 7 \mu\text{m}$. This rough estimate suggests that, at equilibrium for $T < 30$ K and $A < 1000 \mu\text{m}^2$, the BKT crossover is unlikely for this system.

APPENDIX B: SUPERFLUID REGIME FOR POLARITONS

An iterative procedure similar to that developed in this work for the BEC in a trap would be required to properly describe polariton quasicondensation. In this appendix, we give an alternative way of estimating the quasicondensation phase boundary, by making use of the concept of superfluid density. In this way the phase boundary of the normal-superfluid phase transition reported in Fig. 5 has been obtained.

The definition of superfluidity is related to the response of the system under an external perturbation. For the polariton system, this definition is made difficult because an external perturbation can affect very differently the exciton and the photon field. This means that, if only one of the two fields is superfluid, the manifestation of the superfluid (or of the normal) behavior would depend on the kind of perturbation (whether optical or mechanical, for example). Conversely, the system is expected to manifest superfluidity independently on the kind of perturbation, only if both the exciton and the photon superfluid densities are nonvanishing. Here we assume the latter as the proper definition of the superfluid regime for the polariton system.

Our theory allows to compute the exciton and the photon superfluid densities directly via the Landau formula.²³ To this purpose, for the exciton and the photon field we assume a quadratic dispersion characterized by the effective masses m_x and m_c , respectively. We also define the exciton and photon Bogoliubov operators $\hat{\beta}_{\mathbf{k}}$ and $\hat{\alpha}_{\mathbf{k}}$ via

$$\hat{b}_{\mathbf{k}} \equiv u_{\mathbf{k}}^x \hat{\beta}_{\mathbf{k}} + v_{\mathbf{k}}^x \hat{\beta}_{-\mathbf{k}}^\dagger,$$

$$\hat{c}_{\mathbf{k}} \equiv u_{\mathbf{k}}^c \hat{\alpha}_{\mathbf{k}} + v_{\mathbf{k}}^c \hat{\alpha}_{-\mathbf{k}}^\dagger,$$

$$|u_{\mathbf{k}}^{x(c)}|^2 - |v_{\mathbf{k}}^{x(c)}|^2 = 1. \quad (\text{B1})$$

The occupation of the exciton (and photon) Bogoliubov modes is obtained by comparing Eq. (B1) with Eq. (A2). For example, for excitons we have

$$\begin{aligned} \bar{N}_x(E_{\mathbf{k}}) \equiv \langle \hat{\beta}_{\mathbf{k}}^\dagger \hat{\beta}_{\mathbf{k}} \rangle &= [|\Pi_u^x(\mathbf{k})|^2 - |\Pi_v^x(\mathbf{k})|^2] n_B(E_{\mathbf{k}}^{lp}) \\ &+ [|\Omega_u^x(\mathbf{k})|^2 - |\Omega_v^x(\mathbf{k})|^2] n_B(E_{\mathbf{k}}^{up}). \end{aligned} \quad (\text{B2})$$

Within these definitions, the solution of the polariton problem is reformulated in terms of two Bogoliubov problems for the exciton and the photon fields. Therefore, the Landau formula²³ can be used to compute the normal densities of the two species

$$\rho_n^{x(c)} = -\frac{1}{3} \sum_{\mathbf{k}} \hbar^2 k^2 \left. \frac{d\bar{N}_{x(c)}(E)}{dE} \right|_{E_{\mathbf{k}}}. \quad (\text{B3})$$

The superfluid densities are then calculated by subtracting the normal densities to the total ones

$$\rho_s^{x(c)} = m_{x(c)} n_{xx(cc)} - \rho_n^{x(c)}, \quad (\text{B4})$$

where this step is made possible by the quadratic dispersion of the two fields.

The phase boundary of Fig. 5, is computed using the polariton dispersions $E_{\mathbf{k}}^{lp(up)}$, and the corresponding Bogoliubov amplitudes, relative to $A=100 \mu\text{m}^2$ (we have verified that the use of a different area, for example $A=1000 \mu\text{m}^2$ results in negligible quantitative differences). This assumption corresponds to approximating the quasicondensate fraction of the infinitely extended system, with the condensate fraction of a trapped gas.

*davide.sarchi@epfl.ch

¹H. Deng *et al.*, Proc. Natl. Acad. Sci. U.S.A. **100**, 15318 (2003).

²J. Kasprzak *et al.*, Nature (London) **443**, 409 (2006).

³H. Deng, D. Press, S. Gotzinger, G. S. Solomon, R. Hey, K. H. Ploog, and Y. Yamamoto, Phys. Rev. Lett. **97**, 146402 (2006).

⁴R. Balili, V. Hartwell, D. Snoke, L. Pfeiffer, and K. West, Science **316**, 1007 (2007).

⁵J. Keeling, P. R. Eastham, M. H. Szymanska, and P. B. Littlewood, Phys. Rev. Lett. **93**, 226403 (2004).

⁶F. M. Marchetti, J. Keeling, M. H. Szymanska, and P. B. Littlewood, Phys. Rev. Lett. **96**, 066405 (2006).

⁷M. H. Szymanska, J. Keeling, and P. B. Littlewood, Phys. Rev. Lett. **96**, 230602 (2006).

⁸A. Kavokin *et al.*, Phys. Lett. A **306**, 187 (2003).

⁹J. Keeling, Phys. Rev. B **74**, 155325 (2006).

¹⁰F. P. Laussy, G. Malpuech, A. Kavokin, and P. Bigenwald, Phys. Rev. Lett. **93**, 016402 (2004).

¹¹T. D. Doan, H. T. Cao, D. B. Tran Thoai, and H. Haug, Phys. Rev. B **72**, 085301 (2005).

¹²D. Sarchi and V. Savona, Phys. Status Solidi B **243**, 2317 (2006).

¹³P. Schwendimann and A. Quattropani, Phys. Rev. B **74**, 045324

(2006).

¹⁴M. Wouters and I. Carusotto, Phys. Rev. Lett. **99**, 140402 (2007).

¹⁵D. Sarchi and V. Savona, Phys. Rev. B **75**, 115326 (2007).

¹⁶A. Griffin, Phys. Rev. B **53**, 9341 (1996).

¹⁷H. Shi and A. Griffin, Phys. Rep. **304**, 1 (1998).

¹⁸G. Rochat, C. Ciuti, V. Savona, C. Piermarocchi, A. Quattropani, and P. Schwendimann, Phys. Rev. B **61**, 13856 (2000).

¹⁹S. B. de-Leon and B. Laikhtman, Phys. Rev. B **63**, 125306 (2001).

²⁰S. Okumura and T. Ogawa, Phys. Rev. B **65**, 035105 (2002).

²¹I. A. Shelykh, Y. G. Rubo, G. Malpuech, D. D. Solnyshkov, and A. Kavokin, Phys. Rev. Lett. **97**, 066402 (2006).

²²S. Schmitt-Rink, D. S. Chemla, and D. A. B. Miller, Phys. Rev. B **32**, 6601 (1985).

²³L. Pitaevskii and S. Stringari, *Bose-Einstein Condensation* (Oxford University Press, New York, 2003).

²⁴M. D. Lee, S. A. Morgan, M. J. Davis, and K. Burnett, Phys. Rev. A **65**, 043617 (2002).

²⁵R. J. Dodd, M. Edwards, C. W. Clark, and K. Burnett, Phys. Rev. A **57**, R32 (1998).

²⁶M. Holzmann, G. Baym, J.-P. Blaizot, and F. Laloë, Phys. Rev.

- Lett. **87**, 120403 (2001).
- ²⁷N. Prokof'ev, O. Ruebenacker, and B. Svistunov, Phys. Rev. A **69**, 053625 (2004).
- ²⁸Yu. Kagan, V. A. Kashurnikov, A. V. Krasavin, N. V. Prokof'ev, and B. V. Svistunov, Phys. Rev. A **61**, 043608 (2000).
- ²⁹N. Prokof'ev and B. Svistunov, Phys. Rev. A **66**, 043608 (2002).
- ³⁰W. Langbein and J. M. Hvam, Phys. Rev. Lett. **88**, 047401 (2002).
- ³¹M. Richard, J. Kasprzak, R. André, R. Romestain, L. S. Dang, G. Malpuech, and A. Kavokin, Phys. Rev. B **72**, 201301(R) (2005).
- ³²Estimated from a kinetic model (Ref. 15). For this lifetime, also the excitation spectrum should tend to the equilibrium one, as can be seen from Eqs. (8)–(10) of Ref. 14.
- ³³We assume scalar exciton and photon fields. The theory can be generalized to include their vector nature, accounting for light polarization and exciton spin, as done by Shelykh *et al.*, within the Gross-Pitaevskii limit (Ref. 21).
- ³⁴In 2D, many-body correlations affect significantly the two-body scattering amplitude, eventually leading to a vanishing T -matrix at small collision energy and in the thermodynamic limit (Ref. 24). In the HFP approximation, it is then customary to replace the interaction potential $v(\mathbf{k}, \mathbf{k}', \mathbf{q})$ by the many-body T -matrix $T(\mathbf{k}, \mathbf{k}', \mathbf{q}, E)$ obtained from a self-consistent summation of ladder diagrams. Here, we have generalized this approach and computed the many-body T -matrices $T_x(\mathbf{k}, \mathbf{k}', \mathbf{q}, E)$ and $T_s(\mathbf{k}, \mathbf{k}', \mathbf{q}, E)$. We find that, for typical parameters, the correction to v_x and v_s is of only a few percent.
- ³⁵Here we directly plot the function $g^{(1)}(\mathbf{r})$, without introducing any separation into the two contributions associated to phase and density fluctuations, because we refer to conventional BEC in a finite size system. On the other hand, this separation is particularly useful in the presence of quasicondensation. In Appendix A, we separate the two contributions and we discuss under which conditions the typical power-law decay of the spatial coherence could be observed.